tvst

Retina

Characterization of Oxygen Nanobubbles and In Vitro Evaluation of Retinal Cells in Hypoxia

Victoria Messerschmidt[1], Wen Ren[1,2], Michael Tsipursky[3,4], and Joseph Irudayaraj[1,2,4,5]

[1] Biomedical Research Centre (BRC), Mills Breast Cancer Institute, Carle Foundation Hospital, Urbana, IL, USA
[2] Department of Bioengineering, University of Illinois at Urbana-Champaign, Urbana, IL, USA
[3] Vitreo-Retinal Surgery, Ophthalmology Department, Carle Foundation Hospital, Champaign, IL, USA
[4] Carle-Illinois College of Medicine, Champaign, IL, USA
[5] Beckman Institute; Holonyak Micro and Nanotechnology Laboratory; Carl Woese Institute for Genomic Biology, University of Illinois at Urbana-Champaign, Urbana, IL, USA

Correspondence: Joseph Irudayaraj, Department of Bioengineering, 1102 Everitt Lab, 1406 W. Green Street, University of Illinois at Urbana-Champaign, Urbana, IL 61801, USA.
e-mail: jirudaya@illinois.edu

Received: August 23, 2022
Accepted: January 14, 2023
Published: February 10, 2023

Keywords: oxygen nanobubbles; hypoxia; retina; safety and efficacy; treatment

Citation: Messerschmidt V, Ren W, Tsipursky M, Irudayaraj J. Characterization of oxygen nanobubbles and in vitro evaluation of retinal cells in hypoxia. Transl Vis Sci Technol. 2023;12(2):16, https://doi.org/10.1167/tvst.12.2.16

Purpose: Vein or artery occlusion causes a hypoxic environment by preventing oxygen delivery and diffusion to tissues. Diseases such as retinal vein occlusion, central retinal artery occlusion, or diabetic retinopathy create a stroke-type condition that leads to functional blindness in the effected eye. We aim to develop an oxygen delivery system consisting of oxygen nanobubbles (ONBs) that can mitigate retinal ischemia during a severe hypoxic event such as central retinal artery occlusion.

Methods: ONBs were synthesized to encapsulate oxygen saturated molecular medical grade water. Stability, oxygen release, biocompatibility, reactive oxygen species, superoxide, MTT, and terminal uridine nick-end labeling assays were performed. Cell viability was evaluated, and safety experiments were conducted in rabbits.

Results: The ONBs were approximately 220 nm in diameter, with a zeta potential of −58.8 mV. Oxygen release studies indicated that 74.06 µg of O_2 is released from the ONBs after 12 hours at 37°C. Cell studies indicated that ONBs are safe and cells are viable. There was no significant increase in reactive oxygen species, superoxide, or double-stranded DNA damage after ONB treatment. ONBs preserve mitochondrial function and viability. Histological sections from rabbit eyes indicated that ONBs were not toxic.

Conclusions: The ONBs proposed have excellent oxygen holding and release properties to mitigate ischemic conditions in the retina. They are sterile, stable, and nontoxic.

Translation Relevance: ONB technology was evaluated for its physical properties, oxygen release, sterility, stability, and safety. Our results indicate that ONBs could be a viable treatment approach to mitigate hypoxia during ischemic conditions in the eye upon timely administration.

Introduction

Central retinal artery occlusion (CRAO) is akin to an acute stroke in the eye owing to inner retinal ischemia. CRAO constitutes an ophthalmic emergency resulting in irreversible blindness if not treated promptly.[1,2] In humans, a window of opportunity for intervention exists between 24 and 36 hours after the insult. Spontaneous reperfusion occurs in 90% of cases at 72 hours.[3,4] If the patient presents within the treatment window, physicians can prescribe vasodilators, inhalation of 95% oxygen/5% carbon dioxide, hyperbaric oxygen treatment, or thrombolytic therapy, or perform ocular message or laser and anterior chamber paracenesis.[3,5,6] However, clinical studies have not shown evidence that these interventions are effective or can improve visual outcomes in patients.[7]

The incidence rate of CRAO is about 2 in 100,000 person-years, with men more susceptible than women. In the 80 to 84 year age group, cases reach 9.85 per 100,000 person-years.[8] In a global study, of all patients

entering an institution, 6 to 15 patients per year presented with CRAO.[9,10] These patients experienced retinal ischemia, with impaired oxygen metabolism, decreased total retinal blood flow, and diminished oxygen delivery. Experimental ischemia models of the eye have shown that oxygen metabolism is significantly lower than sham experiments.[10–15] Blair et al.[14] introduced graded ischemia in the eye and measured retinal blood flow, oxygen delivery, and oxygen extraction fraction among other measurements that showed even in partial occlusion, there is a potential for retinal damage. Human studies of the eye in those with sickle cell disease,[16] diabetes metellus,[17] and those breathing 12% to 15% oxygen[18] showed decreased oxygen extraction fraction, decreased oxygen metabolism, and decreased oxygen delivery similar to that in Blair et al. These studies have shown that oxygen delivery is critical to normal retinal function, and even slightly hypoxic environments can have a substantial effect on eye health.

The retina is a complex structure with 10 distinct layers. Yu et al.[19] recorded the oxygen metabolism in the following retinal layers: retinal ganglion cells, top and bottom of the inner plexiform layer, and the inner segments. With a lasered occlusion model and a treatment of inhaled oxygen between 20% and 100%, a notable change in oxygen diffusion across the retina as deep as approximately 300 µm, which corresponds with the inner segment of the photoreceptors, was noted.[19] The remaining layers of the retina, from the inner nuclear layer to the retinal ganglion cell and nerve fiber layer remained anoxic.

Nanobubbles (NBs) are formally classified by the ISO 20480–1_2017 as ultrafine bubbles with a diameter of less than 1 µm.[20] NBs can be produced using various materials that are composed of the shell entrapping a gas core.[20,21] The shell interacts with the environment and, therefore, the properties of the shell significantly influence the ability of NBs to be taken up by a cell to elicit a specific response.[21] Additionally, the composition of the shell can affect the half-life, elasticity, shelf-life, and stability of the synthesized NBs.[21] Lipids, polymers, lipid–polymer blends, or proteins are the most common methods of encapsulating gases.[21–23] Lipids are the preferred method of synthesizing NBs because of their biocompatibility, ease of gas release, biodegradability, and ease of ultrasonic vibration.[22,24] Furthermore, lipid shells can be ruptured by ultrasound to enhance oxygen release to the cells.[21] However, lipids alone are unstable and tend to aggregate into larger particles. Polyethylene glycol, cholesterol, or other polymers can be added to stabilize the lipid shell.[21–23] Polymers have been used for NB shell formulation because of their tunable molecular weight, polymer type, and functionalization that can enhance specific properties of the bubbles.[21,25] Proteins used as NB shells are more stable than lipid shells and are able to self-assemble under specific circumstances.[21] NBs with protein shells also allow for limited diffusion,[22] providing a constant release of a therapeutic gas. Other functional proteins, such as avidin or human serum albumin used in Albunex, which has been approved by the US Food and Drug Administration (FDA),[26] can have specialized functionality.[22,24]

Most of the past work involving oxygen entrapped NBs have focused on cancer treatments.[27–41] In addition to NBs being extensively used for imaging in mice,[29,42] other applications include wound healing,[43–45] plasmid delivery in vitro,[21,46] hypoxia mitigation in the recent coronavirus disease 2019 pandemic,[47] and nonmedical applications such as soil aeration,[48] controlling harmful eutrophication,[49] and evaluating plant, fish, and animal growth.[50]

Compared with the NBs described elsewhere in this article, oxygen NBs (ONBs) with the dextran-based shell discussed in this application exhibit unique properties with significant potential to treat retinal ischemia. Dextran is an FDA-approved chemical and enhances the solubility and biocompatibility of the oxygen delivery platform.[51] In this work, we have evaluated the ONBs physical properties and assessed their oxygen release and retention properties. Furthermore, we evaluated the sterility, stability, uptake, cell viability, and mitochondria response in retinal cell cultures. In vivo toxicity was also evaluated in rabbit eyes.

Methods

Dextran ONBs Synthesis

The synthesis of ONBs was conducted per our previously published protocol with modifications[52] to achieve extended oxygen release characteristics and improved stability. Briefly, palmitic acid (P0500-25G, Sigma, St. Louis, MO) was dissolved in a 100% ethanol solution (2701, Decon Laboratories, King of Prussia, PA) and other chemicals were prepared as an aqueous solution. The solutions were then sonicated (SFX 250, Branson, Danbury, CT) under pulse mode with 30 seconds sonication on and 40 seconds sonication off for a total sonication time of 5 minutes at 25% amplitude, total process time of 11 minutes. Before synthesis, 10 mL of biograde water (SH30538.03, Cytiva Life Sciences, Marlborough, MA) was bubbled with pure oxygen for 30 minutes at a pressure of 30 psi to ensure that the water is saturated. To 10 mL of oxygen saturated water under 50% amplitude and oxygenation,

0.2 mL of 0.045% potassium chloride (P9541-500G, Sigma) aqueous solution was added. The obtained solution was subjected to a sonication cycle with 30 seconds on, 40 seconds off, and repeated two times. Then, 0.6 mL of 0.23% Epikuron 170 (DS-Soya PC80-C, Solus Advanced Materials, Seoul, South Korea) was added to the solution and sonicated for 30 seconds on, 40 seconds off for a total of 1 minute of sonication. The following chemicals were added and subsequently sonicated for 2 cycles: 0.4 mL of 0.028% TPGS (D-α-Tocopheryl Polyethylene Glycol Succinate, 57668-5G, Sigma), 1 mL of 0.9% dextran (67578-5G, Sigma), 0.3 mL of 0.19% palmitic acid (P0500-25G, Sigma) and 0.4 mL of 0.4% trehalose (T5251-10G, Sigma). The resulting mixture was sonicated for four more cycles and the obtained ONBs were filtrated with 0.22 µm polyethersulfone membrane filter into a 20-mL glass vial, which was then oxygen saturated and sealed with a rubber stopper and aluminum cap. Parafilm was used to further seal the cap to prevent possible leakage of oxygen.

Fluorescent ONBs (FONBs) were synthesized as noted above, with additional modifications. First, Dextran-FITC (74817, Sigma) was substituted for dextran during the synthesis at a concentration of 9 mg/mL. Additionally, 400 µL of aqueous acridine orange (10 mg/mL, 318337, Sigma) was added to 3.6 mL of ONBs. The bubbles were then dispensed into round bottom tubes and shaken overnight at room temperature at 70 RPM. The following day, the NBs were centrifuged at 50,000$\times g$ for 45 minutes under vacuum. The supernatant was removed, and the ONBs were resuspended in fresh deionized water. The bubbles were centrifuged at the same settings and washed six times to remove unbound acridine orange. The acridine orange–labeled dextran-FITC NBs were stored at 4°C and used within 48 hours.

NB Characterization

The particle diameter and zeta potential of ONBs were evaluated with a Litesizer 500 particle-sizing system from Anton Paar (Ashland, VA). The concentration of ONBs was determined with NanoSight NS300 from Malvern Panalytical (Nottingham, UK) and the TEM image was obtained with a Thermo Fisher FEI Tecnai G2 F20 S-TWIN STEM (Waltham, MA) instrument with an operating voltage at 200 kV.

Measurement of Oxygen in NBs

The oxygen-holding capacity of ONBs was determined in a hypoxia chamber at 37°C and room temperature based on its release. The chamber was purged with nitrogen to decrease the oxygen concentration in the chamber to less than 0.1% within 65 minutes. Deoxygenated water was prepared by bubbling nitrogen into water for 1 hour. The ONBs were mixed with deoxygenated water in a 4:6 ratio and the oxygen concentration in the mixture was monitored with a Thermo Fisher Scientific Orion Versa Star Pro DO Benchtop Meter (Ottawa, Ontario, Canada) fitted with an optical dissolved oxygen probe using the timed measurement model with 1-minute intervals.

Oxygen Release Studies

To track oxygen release from ONBs, a test system simulating an ischemic environment was designed. Briefly, the optical probe was placed in a glass tube 1.7 cm in diameter and sealed with parafilm to isolate the oxygen exchange in the tube and the environment. The ONBs were mixed with deoxygenated water at a 1:9 ratio and the solution was injected into the glass tube and was further sealed with parafilm. The oxygen release was monitored with the dissolved oxygen meter using the timed measurement model at 1-minute intervals.

Effect of pH on ONBs

To assess the effect of pH on oxygen release, the ONBs were mixed with various deoxygenated buffers at 1:9 ratio to obtain mixtures at different pH levels. The measurement method described elsewhere in this article was used for oxygen release studies.

Evaluation of Sterility

Soybean-casein digest media was made following the U.S. Pharmacopeia Sterility <71> recipe. Briefly, casein peptone 1.7 w/v % (R451102, Remel Products, Waltham, MA), Peptone S (soy peptone) 0.3 w/v% (30620061-1, BioWorld, Dublin, OH), sodium chloride 0.5 w/v% (VW6430-1, VWR, Radnor, PA), dibasic potassium phosphate 0.25 w/v % (7088-04, Mallinchrodt Chemicals), and dextrose 0.23 w/v % (G7021-100G, Sigma) were dissolved in 1 L of purified water. The pH was adjusted to 7.3 $\pm$ 0.2 using 1 M NaOH and sterilized via autoclave. ONBs were synthesized the day before the experiment and stored at 4°C overnight. The following day, 9 mL of soybean-casein digest media was added to 1 mL of ONBs in sterile 50-mL tubes. Two additional controls used are biograde water only (1:9 ratio of water:media) and media only. For a positive control, additional 50-mL tubes were directly inoculated with one of the following: *Bacillus subtilis*, *Staphylococcus aureus*,

Pseudomonas aeruginosa 14, Or *Pseudomonas aeruginosa 01*. All samples were incubated at room temperature. The optical density was read with an Eppendorf's BioPhotometer with 1 mL of the sample in a clean cuvette with 1× phosphate-buffered saline (PBS) as a blank. The sample was then returned to the respective 50-mL tube and incubated at room temperature. After 6 days, the bacteria-inoculated samples were pale owing to diminishing nutrients and cell death, and subsequently bleached. Each group had five technical and five biological replicates.

Cell Culture

Muller (ENW001, Kerafast, Boston, MA) and R28 (EUR201, Kerafast) cells were cultured in 5% CO_2 humidified incubator at 37°C. The culture media for Muller cells consisted of DMEM (10–017-CV, Corning, Corning, NY) supplemented with final concentrations of 1% Pen-Strep (17-6020E, Lonza, Basel, Switzerland), 10% fetal bovine serum (16140–071, Gibco, Waltham, MA), and additional 1% L-glutamine (3772, Carl Roth, Karlsruhe, Germany). The culture media for the retinal cell line R28 consisted of the following: DMEM (10-013-CV, Corning) supplemented with 1× MEM nonessential amino acids (11140-050, Gibco), 1% Pen-Strep, 10% bovine calf serum (30–2030, ATCC, Manassas, VA), sodium bicarbonate (15 mL of 7.5 w/v %, 7412-12, Mallinckrodt Chemicals, St. Louis, MO), and L-glutamine (5 mL of 200 mM stock, 3772, Carl Roth). We used 1× PBS to dilute Trypsin-EDTA (25-053-CI, Corning) 1:3 for Muller cells. CMF-EDTA was used as the trypsin dilutant for R28 cells. The recipe for CMF-EDTA was followed as outlined by the R28 care document from Kerafast.

ROS and Superoxide Determination

The ROS and Superoxide Detection assay kit (ab139476, Abcam, Waltham, MA) was used to determine the level of ROS and superoxide after ONBs treatment following the manufacturer's instructions. Briefly, Muller and R28 cells were cultured in a 96-well black-walled, clear bottom plate overnight to ensure attachment. The following day, the cells were treated with ONBs at the following concentrations for 24 hours: 0.1, 0.5, and 1.0 mg/mL of ONBs, and shell at 0.5 mg/mL (no O_2). Additionally, the supplied ROS enhancer, procyanin, was used as the positive control at a concentration of 350 µM, and the included ROS inhibitor N-acetyl-L-cysteine at 5 mM was used as a negative control. Finally, the detection solution was incubated with the cells for 60 minutes at 37°C and read at 488 nm for ROS, and 550 nm for superoxide levels. Each group had a total of eight replicates.

Dark-field Imaging

The uptake of ONBs was evaluated with hyperspectral dark-field microscopy.[53] The cells were cultured on gelatin-coated coverslips for 24 hours for proper adherence. The media was then replaced by buffered FONBs at concentrations of 1.00, 0.75, 0.50, 0.100 mg/mL or no treatment and incubated at 37°C for 4 hours. The slides were then gently washed with 1× PBS and fixed using 3.7% neutral buffered formaldehyde. To identify FONBs, a unique spectral library with FONBs only was created. A standard spectral angle mapper was used to obtain spectra, similar to that of FONBs in treated cells. The estimates were performed with the CytoViva ENVI software.

Cellular Uptake

R28 and Muller cells were cultured in 5% CO_2 humidified incubators at 37°C. At 10,000 cells per well, the cells were grown over night in a 96-well plate to ensure attachment. FONB solution was gently mixed by inversion to ensure homogenous distribution of bubbles. The FONBs were applied to the cells at concentrations of 1.00, 0.75, 0.50, 0.100 or 0 mg/mL for 4 hours at 37°C. The cells were washed three times with 1× PBS to remove unbound FONBs and lysed using 1% triton X-100 to release the uptaken NBs. A FONB standard with various known concentrations was read at 488 nm, and an equation relating FONB concentration to fluorescence intensity was used to measure the number of bubbles that were taken up by the cells. Additionally, the groups were normalized by protein content to compare between cell types using the Pierce BCA Assay by Thermo Fisher Scientific following manufacturer's instructions. By dividing the number of FONBs uptaken by the protein content, the relative amount of FONBs that were taken up was determined.

Cell Viability Studies

Viability Assessment in a Normoxic Environment

R28 and Muller cells were cultured in a 96-well plate at 10,000 cells per well overnight. The following morning, oxygen loaded NBs at 1.00, 0.75, 0.50, 0.10, and 0.50 mg/mL Shell in 1× PBS buffer were added to the cells for a total for 24 hours. After which an MTT (M6494, Invitrogen, Waltham, MA) assay was performed per manufacturer's instructions. Each group had a total of eight replicates.

A terminal uridine nick-end labeling assay (4812-30-K, R&D Systems, Minneapolis, MN) was performed to determine cell death from oxygen-loaded NBs by evaluating double-stranded DNA (dsDNA) breaks following the manufacturer's instructions. Briefly, Muller and R28 cells were cultured on gelatin-coated slides until 80% confluent. Then, ONBs were synthesized and added to each slide at concentrations of 0.1 mg/mL, 0.5 mg/mL, and 1.0 mg/mL or treated with 0.5 mg/mL of the Shell (no O_2). The no treatment (NT) group served as the negative control and cells treated with TACS-nuclease were treated as positive controls. DAPI staining solution (ab228549, Abcam, Cambridge, UK) was used to stain the nuclei following the manufacturer's instructions. DAPI was visualized at 405 nm and dsDNA at 488 nm. Each treatment had two replicates with four images taken per replicate.

Viability Assessment in a Hypoxic Environment

R28 and Muller cells were cultured in a 96-well plate at 10,000 cells per well overnight. The following day, cells were either subjected to normoxic conditions for 6 hours or 6 hours of hypoxia (5% O_2, 5% CO_2, 90% N_2) with the addition of ONBs at 1.00, 0.75, 0.50, or 0.10 mg/mL, shell (no O_2) at 0.5 mg/mL, or no treatment. An MTT assay was the performed per manufacturer's instructions to determine viability. Additionally, cells were normalized via protein content as described previously.

Seahorse Mitochondrial Stress Test

First, R28 and Muller cells were optimized for cell seeding density and carbonyl cyanide P-(trifluromethoxy) phenylhydroazone (FCCP) concentration. FCCP is an uncoupling agent that disrupts the mitochondrial membrane potential. Once administered, the electrons can freely bind to O_2, and the maximal respiration can be measured. FCCP needs to be titrated to measure the maximal respiration without causing toxicity to the cells. Briefly, cells were seeded at 5000, 10,000, 20,000, or 40,000 cells per well and treated with FCCP at 0.5, 1.0, 1.5, or 2.0 µM concentrations. Based on optimization (Supplementary Fig. S1, Supplementary Fig. S2), R28 and Muller cells had optimal readings at 5000 cells/well and treated with 1.5 µM of FCCP.

For NB treatments, R28 and Muller cells were seeded at their optimized density and incubated overnight under normal conditions (5% CO_2, 37°C). The following day, ONBs were added to the cells in groups of 0.75 mg/mL ONBs, 0.50 mg/mL ONBs, 0.10 mg/mL ONBs, 0.75 mg/mL Shell (no O_2), 0.50 mg/mL Shell (no O_2), 0.1 0mg/mL Shell (no O_2), or vehicle only (1× PBS buffer). The cells were then placed in a humidified hypoxia chamber and subjected to 5% CO_2, 5% O_2, and 90% N_2 for 6 hours, after which, the Seahorse Mitochondria Stress Test assay was conducted with the optimized FCCP concentration. Each group had a total of eight replicates. The cell number was quantified by first staining each well with Hoechst and imaged using the DAPI channel on the Cytation 5 Multimode Reader. The imager takes an image of each well and counts the positively labeled cells. The results of the cell count were used in the Wave software for normalization of the Mitochondria Stress Test.

Animal Husbandry and Intravitreal Injection

The following experimental protocol adhered to ARVO's statement for the Use of Animals in Ophthalmic and Vision Research. The study used here was approved by the Institutional Animal Care and Use Committee of the University of Illinois Chicago Pharmacology Department in the Toxicology Research Laboratory following UIC/TRL Study No. 869.

Six male New Zealand white rabbits were housed in an Association for Assessment and Accreditation of Laboratory Animal Care International–accredited facility with a 12-hour light/12-hour dark cycle, fed a high fiber rabbit chow and water ad libitum. The animals were allowed to acclimate for 7 days before injection and randomly placed into two groups. On the day of the procedure, the rabbits were anesthetized with ketamine/xylazine at 30/3 mg/kg and the pupils were dilated using topical 10% phenylephrine and 1% cyclopentolate, followed by a drop of proparacaine hydrochloride 0.5%, and a rinse with sterile saline. A 30G needle was used to inject 25 µL of sterile ONBs solution or saline. After the injections, a triple antibiotic ophthalmic ointment was administered. Intraocular pressure (IOP), body weight, and ophthalmic examinations were conducted at days 0, 3, and 7. After 7 days, the animals were sacrificed and the eye enucleated. The enucleated eyes were stored in ethanol, cryosectioned, and stained with hematoxylin and eosin. An independent observation and examination of the slides was provided by a board-certified veterinarian, Dr Jonathan P. Samuelson (Anatomic) from the Veterinary Diagnostic Laboratory at the University of Illinois at Urbana-Champaign.

Statistical Analyses

Statistical analysis was conducted with R Studio statistical software. For ROS, Superoxide, viability analysis, and mitochondrial stress test, $n = 8$ replicates were evaluated for each cell line. Evaluation of cellular

uptake had an $n = 4$. A one-way analysis of variance followed by a post hoc Tukey test was used to determine statistical differences between groups.

Results

Morphology of the ONB Nanoparticles

The hydrodynamic size of ONBs was measured as 218.71 ± 51.05 nm, whereas the zeta potential was –58.8 ± 1.3 mV. Size distribution of ONBs was recorded as shown in Figure 1A, and Figure 1B shows a typical TEM image of an ONB. The TEM samples of ONBs were stained with 1% uranyl acetate. It can be noted that ONBs are nanospheres with hollow cores as seen from the TEM image (Fig. 1B).

Oxygen Capacity of ONBs Samples

In the hypoxia chamber, the oxygen level that could be maintained can be as low as 0%, so that the ONBs could release all the stored oxygen into the hypoxia chamber. Thus, the oxygen measured in the hypoxia chamber would provide information on the amount of oxygen stored in ONBs. To characterize the total amount of oxygen in ONBs, oxygen release experiments were conducted in the hypoxia chamber at 37°C and room temperature. A solution of freshly prepared ONBs and deoxygenated water at a 4:6 ratio was tested. The change in oxygen concentration over 12 hours was monitored and the results were illustrated in Figure 2. As seen from Figure 2, the oxygen concentration decreases faster at 37°C than at room temperature. A rough calculation was conducted based on the initial and final oxygen concentration in the tested mixture and its volume. It shows that there is approximately 74.06 µg of oxygen released from the test sample containing 7.84 mL of buffer mixture containing 3.14 mL of ONBs solution.

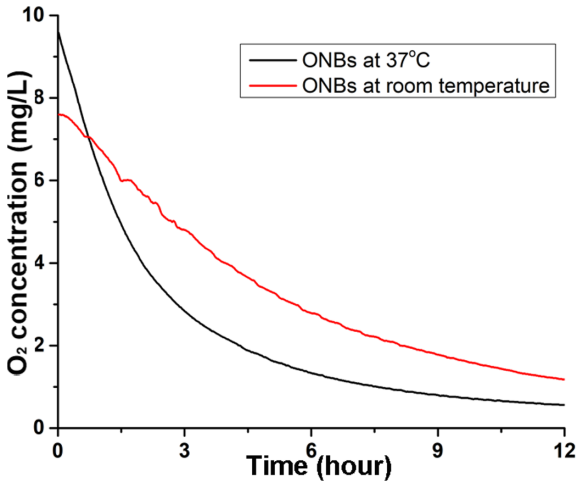

Figure 2. Oxygen release profile at varying temperatures. Oxygen concentration monitoring in hypoxia chamber at 37°C and room temperature of mixtures of ONBs.

Release of Oxygen in NBs

The release of oxygen from ONBs depends on the oxygen concentration gradient across the ONBs shell. To replicate the oxygen release in a hypoxic retina, an isolated system was created where ONBs were injected into deoxygenated water. The oxygen released would then be determined by the difference in oxygen level inside the ONBs and that in hypoxia. When the oxygen concentration across the ONB shell has stabilized, the oxygen release from ONBs would be decreased to a negligible amount owing to the low concentration

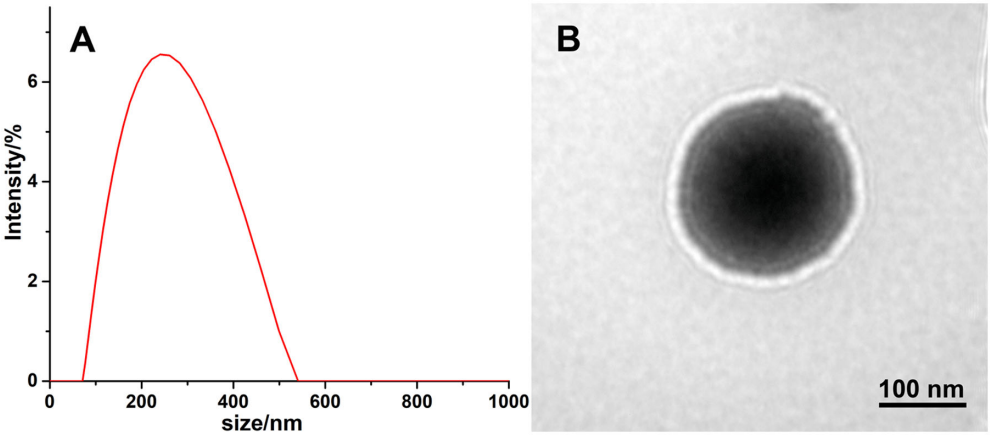

Figure 1. ONB size. Size distribution of ONBs measured by dynamic light scattering (**A**). TEM image of a typical dextran ONB (**B**).

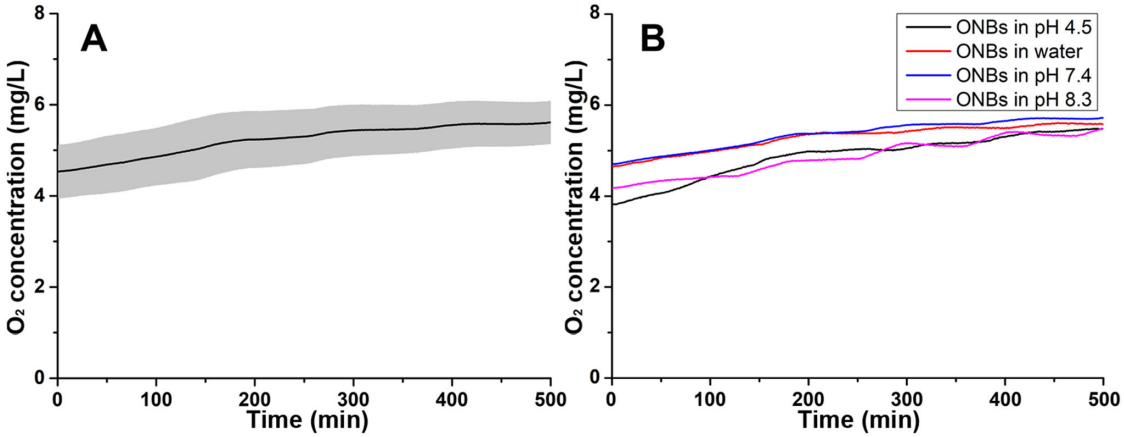

Figure 3. Oxygen release profiles at varying pHs. (**A**) Change in oxygen concentration upon release in isolated hypoxic system. The black line represents the average oxygen concentration, and the grey area depicts the standard deviation from 3 replications. (**B**) Oxygen concentration change with respect to pH. The pH of the sample in water is 7.0.

gradient. To simulate this procedure, a sealed test system was created and the ONBs samples were mixed with deoxygenated water as a model system to evaluate oxygen release. The change in oxygen concentration in the isolated system was recorded to determine the amount of oxygen released from ONBs. Figure 3A shows a typical change in oxygen concentration in the solution of ONBs and deoxygenated water. The oxygen concentration in deoxygenated water is 2.45 ± 0.24 mg/L, whereas the oxygen concentration in the mixture of ONBs and deoxygenated water is 4.53 $\pm$ 0.59 mg/L immediately after the mixing (0 minutes in Fig. 3A). During the experiment, oxygen increased from 4.53 $\pm$ 0.59 mg/L to 5.61 $\pm$ 0.47mg/L after 500 minutes of release in an isolated environment, as shown in Figure 3A. Additionally, separately prepared ONBs were exposed to air for 1 week where the oxygen level in ONBs samples were in equilibrium with that of air. The exposed NBs were tested, and the concentration of oxygen was estimated as 3.29 ± 0.12 mg/L (data not shown). Therefore, the higher concentration of oxygen in the ONBs should be attributed to the oxygen stored in the ONBs.

Effect of Buffers on ONB Release Profile

The pH of the environment is critical for oxygen release studies since the OH ions may interact with the components of the shell of ONBs to result in a change in zeta potential,[24,25] and, therefore, its physical properties. The oxygen release characteristics of ONBs was evaluated in various pH conditions to assess stability, and the results are shown in Figure 3B. In the pH range of 4.5 to 8.3, the difference in oxygen concentration was not significant. Meanwhile, the oxygen release of ONBs in water (pH 7.0) was similar to other mixtures made with deoxygenated buffer, suggesting that the ionic strength of the solution would not influence the oxygen release properties of ONBs.

Sterility of ONBs

After the US Pharmacopeia Sterility Tests <71>, the sterility of NBs was investigated.[54] After the first day, obvious bacterial growth was noted in the *B subtilis*, *P aeruginosa 14*, *P aeruginosa 01*, and *S aureus* positive control samples. After 6 days, the bacteria samples were terminated owing to the lowering of optical density, indicating cell death. During this time, the NB samples continued to show no bacterial growth, and were visually clear throughout the testing timeline (Fig. 4A).

Owing to the nature of oxygen and hypoxic environments, the potential of ONBs to form reactive oxygen species (ROS), or, more specifically superoxide, was assessed. The various concentration of NBs tested in Muller and R28 cells had significantly lower ROS and superoxide levels compared with the positive control, pyocyanin ($P < 0.0001$) (Figs. 4B, 4C). Additionally, the difference between the negative control, ROS inhibitor N-acetyl-L-cysteine, and ONBs at the evaluated concentrations was not statistically significant. These results show that ONBs do not induce ROS or, more specifically, superoxide.

Cell Viability and Uptake

In this experiment, the uptake of ONBs by different retinal cells were evaluated. Muller cells have been shown to contain mannose receptors,[55] whereas

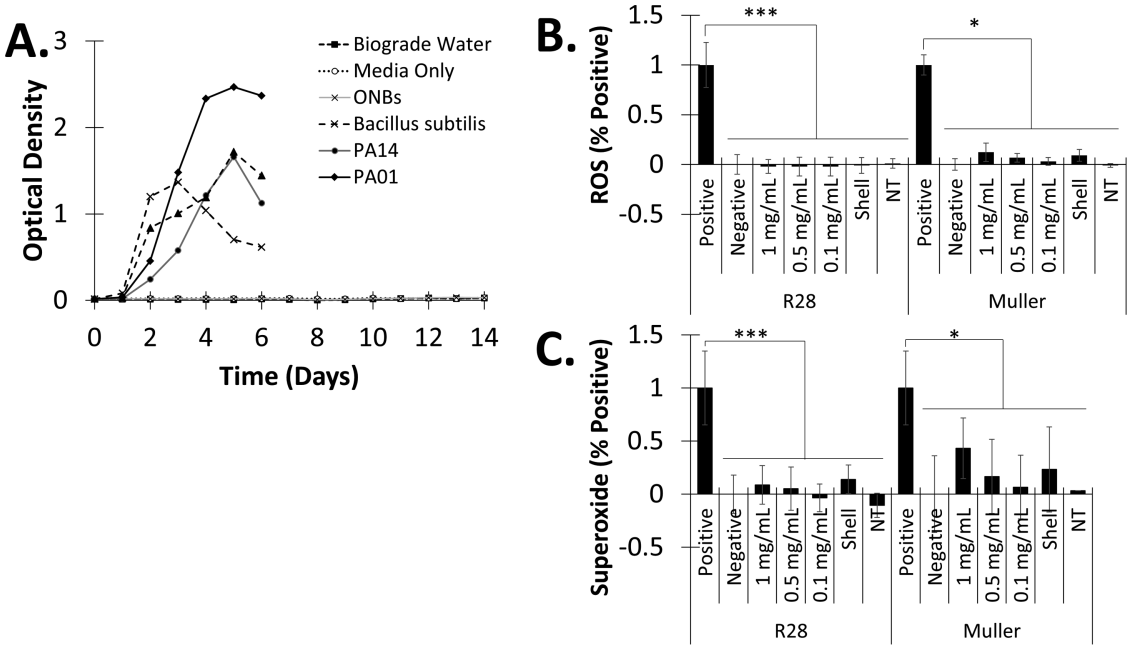

Figure 4. Sterility and ROS evaluation in retinal cells. (**A**) Optical density of NBs in the soybean-casein digest media with bacteria over time ($n = 5$). (**B**) ROS generation after exposure to R28 and Muller cells with different concentration of ONBs ($n = 8$). (**C**) Superoxide levels in retinal cells after treatment ($n = 8$). NT, no treatment; Negative control, *N*-acetyl-L-cysteine; Positive control, pyocyanin. All data shown as mean ± standard deviation. ***$P < 0.0001$; *$P < 0.05$.

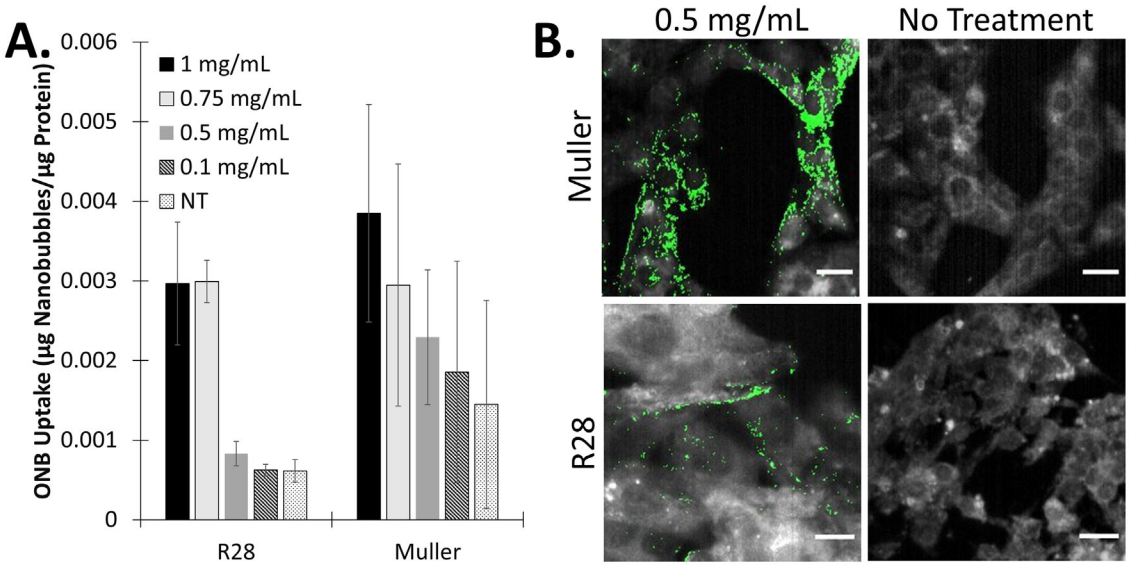

Figure 5. Uptake of ONBs by retinal cells. (**A**) Quantitative representation of fluorescent acridine orange labeled ONBs ($n = 4$). NT, No treatment. All data are represented as the mean ± standard deviation. (**B**) Darkfield images of Muller cells and R28 cells. Cellular uptake of fluorescent NBs (green). Scale bar, 10 µm. Original magnification ×40.

R28 cells contain neuron- or glial-like receptors, but a highly diminished or absence of mannose receptors.[56–58] Although the main mechanism of nanoparticle uptake was via clatherin-dependent endocytosis,[55,59] the clustering of mannose receptors by the NBs is expected to induce endocytosis leading to a higher uptake of NBs.[59] The uptake of ONBs was found to be dose dependent (Fig. 5A), indicating that the NBs will continue to uptake ONBs in a dose-dependent manner to allow for a higher dose based on oxygen needed. In Figure 5B, dark-field images of ONBs in retinal cells are provided and show the uptake in Muller

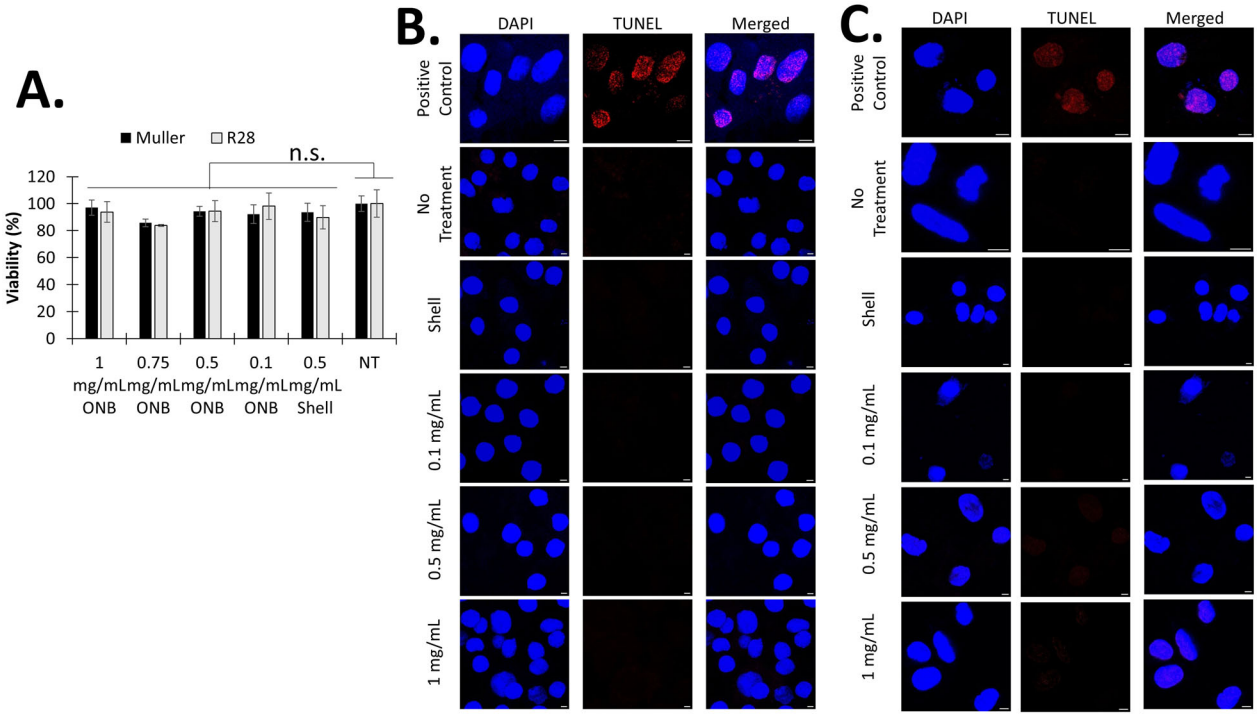

Figure 6. Viability of retinal cells post NB treatment. (**A**) MTT Viability assay of R28 and Muller cells after treatment with oxygen loaded NBs for 24 hours in normoxia. NT, No treatment. Data are shown as the mean ± standard deviation ($n = 8$). Representative images of terminal uridine nick-end labeling assay of Muller cells (**B**) or R28 cells (**C**) after 24 hours of exposure of O_2-loaded NBs at 0.1 mg/mL, 0.5 mg/mL, 1 mg/mL, Shell at 0.5 mg/mL (no O_2), no treatment, and positive control of TACS-nuclease treated cells. Scale bar, 5 µm.

cells was greater than R28 cells. Oxygen-loaded dextran NBs were added to Muller and R28 cells and viability assessed after 24 hours. Cell viability experiments were assessed by MTT assay (Fig. 6A), and DNA damage with terminal uridine nick-end labeling assay (Figs. 6B, 6C). The MTT assay indicates that there was no significant cell death for the different concentrations tested compared with nontreated cells at normoxic conditions. Supporting this finding, we found that there is no dsDNA breakage in the Muller and R28 cells, indicating that the ONBs are safe.

To test for the efficacy of ONBs in vitro, Muller and R28 cells were kept in a hypoxic chamber for 6 hours to evaluate its potential to rescue cells in hypoxia. The MTT assay indicated that the 0.1 mg/mL ONB, 0.5 mg/mL ONB, and the shell significantly lower cell viability compared with the NT normoxia Muller cells and, therefore, was not effective in rescuing the cells from hypoxia. The dose of 1.00 and 0.75 mg/mL of ONBs was able to sustain Muller cells and had increased viability similar to that of Muller cells at normoxic conditions (Fig. 7). When R28 cells were treated with 1 mg/mL of ONBs, the cell viability was significantly greater than no treatment in hypoxia. However, 1 mg/mL of ONBs was not able to increase the cell viability of R28 cells to the same level as that of normoxic conditions. All other concentration of ONBs in R28-treated cells were found to be statistically different from normoxic conditions, indicating that there was no increase in viability. In both cell types, there was a significant dose-dependent response to the ONBs (Fig. 7). For R28 cells, in general, the viability was lower compared with Muller cells when treated with ONBs under hypoxic conditions.

R28 and Muller cells were subjected to hypoxia (5% O_2, 5% CO_2, 90% N_2) for 6 hours and mitochondrial health was evaluated. From the optimization experiments, the mitochondrial respiration output was compared with the typical mitochondrial stress profile (Supplementary Fig. S1A). The FCCP and cell seeding concentration was determined based on the oxygen consumption rate. The group with similar starting oxygen consumption rate values and the highest maximal respiration plateau was chosen as the optimized FCCP for cell seeding (Supplementary Figs. S1B, S1C, S1D, S2). From the optimization experiments, the optimal concentrations for both the R28 and Muller cells were 5000 cells/well and the concentration of FCCP was 1.5 µM (Supplementary Figs. S1, S2). The cells were then incubated in hypoxia for 6 hours with the addition of 0.10, 0.50, 0.75 mg/mL of oxygen-loaded NBs, 0.10, 0.50, 0.75 mg/mL

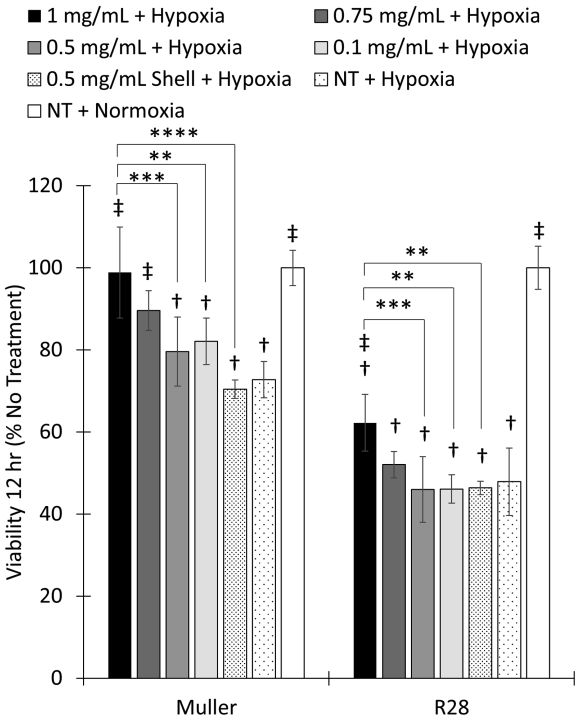

Figure 7. Viability of retinal cells in hypoxia with ONBs. Muller and R28 retina cell viability after 6 hours in hypoxia (5% O_2) with varying concentrations of NBs or no treatment. Shell (no O_2) groups were treated with a concentration of 0.5 mg/mL. Data are shown as mean ± standard deviation. NT, no treatment. † Significant difference to NT Normoxia. ‡ Significant difference to NT hypoxia ($n = 8$). ****$P < 0.00001$; ***$P < 0.0001$; **$P < 0.001$.

of shells (no O_2), or no treatment and the maximal mitochondrial respiration was measured from the Seahorse Mitochondrial Stress Test. Hypoxia causes ROS to form, which ultimately damages the mitochondria of the cells, potentially resulting in lower respiration efficiency. The mitochondrial damage decreases the maximal respiration as evaluated by the Seahorse assay. It is shown that the ONBs have a significant effect on maximal respiration compared with untreated cells (Fig. 8). In the Muller and R28 cells, the ONB groups had a significantly higher maximal respiration compared with the no treatment groups (Fig. 8). Additionally, in the Muller cells there was a significant dose-dependent response indicating a higher ONBs concentration contributes to greater protection of the mitochondria during hypoxia.

Safety of ONBS In Vivo

Rabbits were evaluated 7 days after intravitreal injection. At the time of evaluation, there were no clinical signs of toxicity during gross examination. General ophthalmic examinations revealed no signs of ocular toxicity in all the animals tested, regardless of the group (Supplementary Table S2). Additionally, there was no change in body weight (Supplementary Table S1) or change in the IOP (Fig. 9A, Supplementary Table S3). The cornea and conjunctiva, anterior chamber and iridocorneal angle, anterior uvea, lens, posterior and

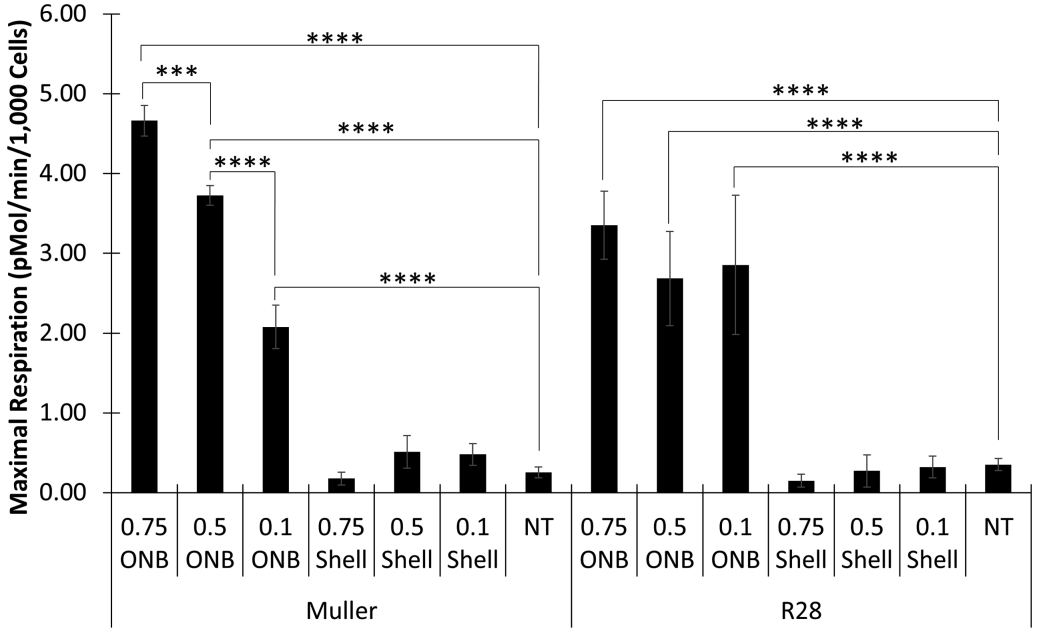

Figure 8. Maximal mitochondria respiration after hypoxia and ONB treatment. After exposing R28 and Muller cells to 6 hours of hypoxia with three concentrations of oxygen-loaded dextran NBs, a dose-dependent protection of mitochondria maximal respiration was observed. Cells were seeded at 5000 cells/well and treated with an FCCP concentration of 1.5 µM. NT, no treatment. Data are shown as the mean ± standard deviation, with $n = 8$. ****$P < 0.00001$; ***$P < 0.0001$.

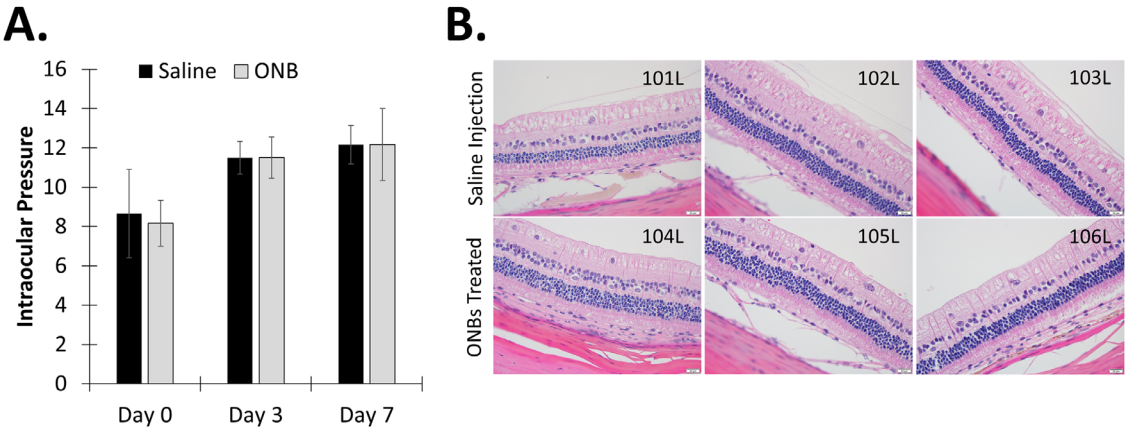

Figure 9. Safety of ONB in vivo. (**A**) Change in the IOP of rabbit eyes after injection of saline or ONBs. Data shown as mean ± standard deviation with n = 6. (**B**) Representative images of rabbit retinas 7 days after injection. Rabbits were intravitreally injected with either saline (top: 101L, 102L, 103L) or ONBs (bottom: 104L, 105L, 106L). Scale bar, 20 µm. Original magnification ×40.

vitreous chambers, choroid and retina, sclera and optic nerve, and orbital tissue were all examined and found to have no abnormalities (data not shown). In the retina, there were no noted abnormalities (Fig. 9B). Last, although there was an increase in IOP after injection, there was no significant difference in IOP between the saline and ONBs groups at any stage (Fig. 9A).

Discussion

NBs have been proposed as a potential treatment to mitigate cancer hypoxia and as an imaging agent.[22,27–42] Recently, ONBs have been shown to rescue cells and tissues from hypoxia owing to their ability to deliver oxygen to the hypoxic regions in chronic wounds in vitro[43,44] and in vivo[45] and proposed as a possible treatment for coronavirus disease 2019.[47] In ophthalmology, NBs have been researched as a delivery agent to the retina in vitro,[60] as well as in bovine and porcine explanted eyes.[61] Herein, we propose an ONBs formulation that is sterile, stable, and safe to treat retinal hypoxia during an ischemic event, such as CRAO.

NBs are spherical particles with an outer shell and an inner gas core, which are tunable during synthesis. Many substances, such as liposomes and synthetic or natural polymers, have been used to entrap gases, drugs, and other payloads.[21,62] The innate characteristics of the shells will determine the pharmacokinetics, stability, efficiency, and release of the payload. An in-depth review of NBs as drug delivery vehicles is provided elsewhere.[22,63,64]

The ONBs synthesized were found to have a hydrodynamic diameter of 218.71 ± 51.05 nm. Many other investigators have used perfluorocarbons owing to their ability to dissolve large amounts of oxygen[37,38,65,66] and the reported size of the NBs varied between 160 and 860 nm.[37,38,66,67] This wide range confirms our findings and depicts the vast range of NB sizes. There are few similar dextran-shelled NBs, which reported sizes of 590.00 nm,[68] 348.45 ± 7.30 nm,[69] 596.35 ± 194.09 nm,[70] and 486.87 ± 147.62 nm.[71] Compared with the NBs synthesized here, other dextran-shelled NBs are larger with wider standard deviations. The zeta potential values reported were –25.00 mV,[68] –53.27 ± 5.96 mV,[69] –25.68 ± 1.00 mV,[70] and –27.31 ± 1.00 mV.[71] The ONBs produced here had a similar zeta potential of –58.8 ± 1.3 mV. The small changes in the shell excipients could contribute to the changes in both the size and zeta potential.

When perfluorocarbons were used to store oxygen, the release profiles yielded 10 mg/L,[38] 30 mg/L,[37] or 6 mg/L[72] of oxygen. Other's reported dextran NBs showed 0.43 ± 0.01 mg/mL of oxygen[71] or 4.573 mg/mL.[52] Comparing the moles of oxygen released per liter, the ONBs synthesized here released similar amounts of oxygen to that of other dextran-based NBs.[52,71] Even though perfluorocarbons allow more oxygen to dissolve, the ONBs had similar release compared with two other reported perfluorocarbon-based, oxygen-loaded NBs (Table 1).[37,38] However, the synthesis methods used in this work are faster, contain excipients that are FDA approved or marked as Generally Regarded as Safe, easier to scale up, and, most important, safe for the retina.

To determine whether the ONBs were endocytosed or simply released oxygen into the surrounding media, the ONBs were incubated with retinal cells. From our experiments, the cells incubated with ONBs were taken up in a dose-dependent manner (Fig. 5A) as visualized

Table 1. Properties of ONBs and Oxygen Release Characteristics

Reported Oxygen Release	Shell Material	Perfluorocarbon Used	Oxygen Released (μmol O_2/L Bubbles)	Size (nm)	Reference
5.61 ± 0.47 mg O_2/L	Dextran	None	156.34	218.71 ± 51.05	–
3000 nL O_2/μL	Dextran	None	134.05	119.6 ± 44.9	Fayyaz 2021[52]
4.5 mg/L	Dextran	Perfluoropentan	140.71	550 ± 30	Cavalli 2009[73]
0.43 ± 0.01 mg O_2/mL	Dextran	Perfluoropentane	134.45	486.87 ± 147.62	Prato 2015[71]
6 mg O_2/L	RBCs	1-bromohepta-decafluorooctane	938.08	130	Zhuge 2022[72]
8.5 mg O_2/L	DSPC, DPPG, DSPG-PEG lipid with PEG	1H-1H perfluoro-octan-1-ol	312.69	263.2 ± 10.3	Song 2018[38]
30 mg O_2/L	C18PMH-PEG	Perfluorohexane	187.62	193	Song 2017[37]

PEG = Polyethylene glycol.

with dark field imaging (Fig. 5B). Others' using dextran as the main shell material did not quantitatively estimate NB uptake. In general, the Muller cells have a higher uptake of ONBs compared with R28 cells, shown both quantitatively and qualitatively (Fig. 5). It has also been demonstrated that dextran, the main chemical constituent of the ONBs synthesized in this work, can interact with mannose receptors on cells.[59,74] Because Muller cells have a higher expression of mannose receptors[55] and the R28 cells lack thereof,[56] Muller cells were noted to readily uptake ONBs. Although R28 cells do uptake the ONBs, the uptake rate is much slower. When dextran particles bind to mannose receptors, the cell membrane begins to cluster around the bound particle, and subsequently facilitates endocytosis.[59] It is suggested that the binding of ONBs to the mannose receptors on the cells could contribute to an increase in cellular uptake that could potentially affect treatment efficacy.

To ensure that ONBs do not adversely affect cell function and safety, sterility, ROS, and superoxide levels were evaluated. The NBs, water, and media groups were all statistically similar in the sterility study and showed no bacterial growth for more than 14 days. Additionally, there were significantly lower ROS and superoxide levels than their respective positive controls (Figs. 4B, C), indicating that ONBs do not contribute to ROS generation. There is a slight increase in ROS and superoxide in Muller cells. Jones et al.[74] suggested that dextran binds to mannose receptors to block tissue plasminogen factor uptake in rat liver endothelial cells. However, only larger molecular weight dextran causes the cell membrane to cluster around the dextran. Additionally, Broderick et al.[55] showed that retinal microglia had mannose receptor-mediated uptake of dextran-FITC, which is considered to be clathrin-mediated endocytosis.[59] The increase in ONBs uptake could correlate with an increase in ROS and superoxide detected. Previously published work on ONBs have shown that these are well-tolerated, but do not indicate whether the addition of oxygen causes ROS species to be produced.[52,71,75] The exception was when oxygen was supplied to create ROS species to enhance photodynamic therapy.[72,76]

Next, the viability of cells exposed to various concentrations of ONBs was evaluated. At all tested concentrations, no significant difference was observed between the NT and the dextran shell concentrations (Fig. 6A). Last, the ONBs were stained for dsDNA damage. Figures 6B and 6C depict that there was no dsDNA damage at all of the concentrations tested in both Muller and R28 cell lines.

After determining that the ONBs are not toxic to the retinal cells, the efficacy of the bubbles was tested. The ONBs were able to successfully provide a viable environment for Muller cells to grow, when subjected to a hypoxic environment. The NT hypoxia, 0.1 mg/mL, 0.5 mg/mL, and all shell concentrations were found to be significantly different from NT Normoxia, indicating that these concentrations did not improve the viability of Muller cells. The 1.00 and 0.75 mg/mL ONB treatments were found to be significantly different from the no treatment hypoxia, and, therefore, contributed to improving cell viability. Additionally, both 1.00 and 0.75 mg/mL were found to be not significantly different from the NT normoxia group. This indicates that the 1.00 and 0.75 mg/mL dosage of

ONBs was sufficient to sustain cell growth in hypoxia that is similar to that of cell growth in normoxic conditions of Muller cells for 6 hours (Fig. 7). Comparing the shell and ONBs, one can understand that it is the oxygen loaded in the ONBs that contributes to the improved viability, and not the shell components. The increase in cell viability could be due to the higher uptake related to the increased number of mannose receptors.[55,56,58,74] Importantly, a dose-dependent response to the ONBs was observed, which could allow higher concentrations of oxygen to be delivered by increasing the amount of ONBs.

In the R28 cells, a similar dose-dependent trend was also noted, where the higher the ONB concentration, the higher the cell viability. All tested concentrations of ONBs were found to be significantly different from the NT normoxia, indicating that all groups had a significantly lower cell viability. However, the 1 mg/mL dose of ONBs exhibited a significantly higher viability compared with untreated cells in hypoxia, indicating that the ONBs were able to successfully provide oxygen to improve cell viability, but that oxygen for the doses evaluated was not sufficient to return the R28 cells to 100% viability.

It was shown that the ONBs can release oxygen for up to 8 hours (Fig. 3). However, as the in vitro hypoxic microenvironment becomes more acidic over time, owing to cells converting from aerobic to anaerobic respiration, the pH decreases and a change in the oxygen release profile of the ONBs will be observed similar to Figure 4. The change in environment and, thus, the oxygen release profile, combined with an increase in the oxygen extraction fraction in hypoxia,[10,11,13,15] will consume a higher percentage of available oxygen released by ONBs. Cells exposed to hypoxia for 6 hours and treated with ONBs could be rescued.

Muller and R28 cells treated with ONBs in a hypoxic environment for 6 hours showed a significantly higher maximal respiration than those exposed to hypoxia alone (Fig. 8). In both the Muller and R28 cell lines, there was a significant increase in maximal respiration in all ONB-treated groups. All shell groups had no significant difference compared with the NT group, which implies that the oxygen supplied by the ONBs protects the mitochondria. Additionally, the Muller cells showed a significant dose-dependent response where an increase in ONBs concentration corresponded with an increase in mitochondrial maximal respiration. In R28 cells, there was no significant dose-dependent response. This finding could be attributed to the higher expression of mannose receptors and uptake of the ONBs discussed elsewhere in this article. This additional information supports the hypothesis that the ONBs are able to preserve the cells during an ischemic event.

New Zealand White rabbits were injected with saline (controls) or ONBs to determine acute ophthalmic toxicity. There were no clinical differences in body weight or general clinical signs (Supplementary Tables S1, S2). Additionally, there was no significant change in IOP between the saline control and the ONBs injections at any time (Fig. 9A). Most significantly, there were no negative ophthalmic signs of injury (Supplementary Table S3) upon examination by a board-certified veterinarian. At 7 days after injection, the retina did not show any decrease in visual acuity between the treatment and control groups (Fig. 9B). Our in vivo study shows that after injecting the maximal dose of 25 µL of ONBs, there were no observable toxicity to the overall rabbit health, especially the eye.

The ONBs synthesized show excellent controlled release properties, releasing oxygen over a 12-hour period in the anoxic environment. Additionally, the ONBs were safe and were readily taken up by retinal cells. Notably, the ONBs were able to significantly increase the viability of Muller and R28 cells in hypoxia. Seahorse experiments to assess mitochondrial health indicated that both Muller and R28 cells in hypoxia had significantly higher mitochondrial maximal respiration upon ONBs treatment compared with the NT group. In vivo toxicity tests showed no differences in clinical signs, ophthalmic examinations, or retinal health in rabbits injected with either saline or ONBs. Further animal ischemia models such as laser vascular occlusion model and carotid occlusion model will be used, which closely replicate human retinal ischemia.

The ONBs described here are not limited to retinal diseases alone. Other potential applications have been demonstrated in chronic wound healing,[44,45,71,77] hypoxemia, and in treating hypoxia in cancer.[22,28,29,31,33–36,38–40,73,78] For ophthalmic diseases, the ONBs could be injected via a standard aseptic pars plana intravitreal injection technique using a 30G needle, which is performed routinely in ophthalmology offices. Currently, for CRAO there is no proven efficacious treatment, thus our intervention could be highly relevant. For more chronic ischemic ocular conditions such as retinal vein occlusions and diabetic retinopathy, the ONBs can potentially serve as an adjuvant to intraocular anti-vascular endothelial growth factor treatment and intraocular steroids. The treatment will be useful any time during the 36-hour window. However, time-dependent ischemic damage could occur and the efficacy of ONBs likely to be lower, when applied beyond the treatment threshold window.

Ischemic optic neuropathy and neurotrophic keratitis are other conditions in the eye that may benefit from the ONBs described herein. Overall, ONBs described in this work have extended oxygen release properties, are nontoxic, and have the potential to rescue retinal cells from hypoxia and hence can be a promising treatment option to rescue the retina from an ischemic insult.

Acknowledgments

The authors thank Jonathan P. Samuelson DVM, MS, DACVP at the University of Illinois College of Veterinary Medicine for evaluation of the stained rabbit retinas. Rabbit toxicology study was conducted at the Toxicology Research Laboratory at the University of Illinois, Chicago. The authors also thank Steven Roth at UIC (University of Illinois, Chicago) for the insightful discussions.

Partial funding for this work was provided by the NSF SBIR Phase I grant (Award# 2032323) to ReVive Biotechnology LLC, with subaward to UIUC, and the Mikashi Award from the Carl Woese Institute for Genomic Biology at UIUC.

Disclosure: **V. Messerschmidt,** EnterpriseWorks, University of Illinois at Urbana-Champaign; **W. Ren,** University of Illinois at Urbana-Champaign; **M. Tsipursky,** ReVive Biotechnology LLC, and Carle Foundation Hospital; **J. Irudayaraj,** University of Illinois at Urbana-Champaign

References

1. Youn TS, Lavin P, Patrylo M, et al. Current treatment of central retinal artery occlusion: a national survey. *J Neurol*. 2018;265(2):330–335, doi:10.1007/s00415-017-8702-x.
2. Varma DD, Cugati S, Lee AW, Chen CS. A review of central retinal artery occlusion: clinical presentation and management. *Eye (Lond)*. 2013;27(6):688–697, doi:10.1038/eye.2013.25.
3. Cugati S, Varma DD, Chen CS, Lee AW. Treatment options for central retinal artery occlusion. *Curr Treat Options Neurol*. 2013;15(1):63–77, doi:10.1007/s11940-012-0202-9.
4. Mac Grory B, Schrag M, Biousse V, et al. Management of central retinal artery occlusion: a scientific statement from the American Heart Association. *Stroke*. 2021;52(6):e282–e294, doi:10.1161/STR.0000000000000366.
5. Tobalem S, Schutz JS, Chronopoulos A. Central retinal artery occlusion - rethinking retinal survival time. *BMC Ophthalmol*. 2018;18(1):101, doi:10.1186/s12886-018-0768-4.
6. Hayreh SS, Zimmerman MB, Kimura A, Sanon A. Central retinal artery occlusion. *Exp Eye Res*. 2004;78(3):723–736, doi:10.1016/s0014-4835(03)00214-8.
7. Schrag M, Youn T, Schindler J, Kirshner H, Greer D. Intravenous fibrinolytic therapy in central retinal artery occlusion: a patient-level meta-analysis. *JAMA Neurol*. 2015;72(10):1148–1154, doi:10.1001/jamaneurol.2015.1578.
8. Kim J, Byun SJ, Woo SJ, Park KH, Park SJ. Assessment of trends in the incidence rates of central retinal artery occlusion in Korea from 2002 to 2015. *JAMA Ophthalmol*. 2021;139(4):399–405, doi:10.1001/jamaophthalmol.2020.6860.
9. Thangamathesvaran L, Miller SC, Tsou B, et al. Global current practice patterns for the management of central retinal artery occlusion. *Ophthalmol Retina*. 2022;6(5):419–434, doi:10.1016/j.oret.2022.01.014.
10. Matei N, Leahy S, Auvazian S, Thomas B, Blair NP, Shahidi M. Relation of retinal oxygen measures to electrophysiology and survival indicators after permanent, incomplete ischemia in rats. *Transl Stroke Res*. 2020;11(6):1273–1286, doi:10.1007/s12975-020-00799-9.
11. Karamian P, Burford J, Farzad S, Blair NP, Shahidi M. Alterations in retinal oxygen delivery, metabolism, and extraction fraction during bilateral common carotid artery occlusion in rats. *Invest Ophthalmol Vis Sci*. 2019;60(8):3247–3253, doi:10.1167/iovs.19-27227.
12. Leahy S, Farzad S, Blair NP, Shahidi M. Retinal oxygen delivery, metabolism, and extraction fraction during long-term bilateral common carotid artery occlusion in rats. *Sci Rep*. 2020;10(1):10371, doi:10.1038/s41598-020-67255-4.
13. Blair NP, Tan MR, Felder AE, Shahidi M. Retinal oxygen delivery, metabolism and extraction fraction and retinal thickness immediately following an interval of ophthalmic vessel occlusion in rats. *Sci Rep*. 2019;9(1):8092, doi:10.1038/s41598-019-44250-y.
14. Blair NP, Felder AE, Tan MR, Shahidi M. A model for graded retinal ischemia in rats. *Transl Vis Sci Technol*. 2018;7(3):10, doi:10.1167/tvst.7.3.10.
15. Teng PY, Wanek J, Blair NP, Shahidi M. Inner retinal oxygen extraction fraction in rat. *Invest Ophthalmol Vis Sci*. 2013;54(1):647–651, doi:10.1167/iovs.12-11305.
16. Shahidi M, Felder AE, Tan O, Blair NP, Huang D. Retinal oxygen delivery and metabolism in healthy

and sickle cell retinopathy subjects. *Invest Ophthalmol Vis Sci*. 2018;59(5):1905–1909, doi:10.1167/iovs.17-23647.
17. Fondi K, Wozniak PA, Howorka K, et al. Retinal oxygen extraction in individuals with type 1 diabetes with no or mild diabetic retinopathy. *Diabetologia*. 2017;60(8):1534–1540, doi:10.1007/s00125-017-4309-0.
18. Palkovits S, Told R, Schmidl D, et al. Regulation of retinal oxygen metabolism in humans during graded hypoxia. *Am J Physiol Heart Circ Physiol*. 2014;307(10):H1412–H1418, doi:10.1152/ajpheart.00479.2014.
19. Yu DY, Cringle SJ, Yu PK, Su EN. Intraretinal oxygen distribution and consumption during retinal artery occlusion and graded hyperoxic ventilation in the rat. *Invest Ophthalmol Vis Sci*. 2007;48(5):2290–2296, doi:10.1167/iovs.06-1197.
20. ISO 20480-1_2017(en). Fine bubble technology — general principles for usage and measurement of fine bubbles — part 1: terminology. 2017. Available: https://www.iso.org/standard/68187.html.
21. Cavalli R, Bisazza A, Lembo D. Micro- and NBs: a versatile non-viral platform for gene delivery. *Int J Pharm*. 2013;456(2):437–445, doi:10.1016/j.ijpharm.2013.08.041.
22. Khan MS, Hwang J, Lee K, et al. Oxygen-carrying micro/nanobubbles: composition, synthesis techniques and potential prospects in photo-triggered theranostics. *Molecules*. 2018;23(9):2210, doi:10.3390/molecules23092210.
23. Batchelor DVB, Armistead FJ, Ingram N, et al. Nanobubbles for therapeutic delivery: Production, stability and current prospects. *Curr Opin Colloid Interface Sci*. 2021;54:101456, doi:10.1016/j.cocis.2021.101456.
24. Sirsi S, Borden M. Microbubble compositions, properties and biomedical applications. *Bubble Sci Eng Technol*. 2009;1(1–2):3–17, doi:10.1179/175889709X446507.
25. Chatterjee M, Chanda N. Formulation of PLGA nano-carriers: specialized modification for cancer therapeutic applications. *Mater Adv*. 2022;3(2):837–858, doi:10.1039/d1ma00600b.
26. Christiansen C, Kryvi H, Sontum PC, Skotland T. Physical and biochemical characterization of Albunex, a new ultrasound contrast agent consisting of air-filled albumin microspheres suspended in a solution of human albumin. *Biotechnol Appl Biochem*. 1994;19(3):307–320.
27. McEwan C, Owen J, Stride E, et al. Oxygen carrying microbubbles for enhanced sonodynamic therapy of hypoxic tumours. *J Control Release*. 2015;203:51–56, doi:10.1016/j.jconrel.2015.02.004.
28. Bhandari P, Lei O, Irudayaraj J. Hypoxia re-programming oxygen nanobubbles sensitize human glioblastoma cells to temozolomide via methylation alterations. *J Bionanosci*. 2017;11(5):337–345, doi:10.1166/jbns.2017.1450.
29. Bhandari P, Novikova G, Goergen CJ, Irudayaraj J. Ultrasound beam steering of oxygen nanobubbles for enhanced bladder cancer therapy. *Sci Rep*. 2018;8(1):3112, doi:10.1038/s41598-018-20363-8.
30. Bhandari PN, Cui Y, Elzey BD, Goergen CJ, Long CM, Irudayaraj J. Oxygen nanobubbles revert hypoxia by methylation programming. *Sci Rep*. 2017;7(1):9268, doi:10.1038/s41598-017-08988-7.
31. Cavalli R, Bisazza A, Rolfo A, et al. Ultrasound-mediated oxygen delivery from chitosan nanobubbles. *Int J Pharm*. 2009;378(1–2):215–217, doi:10.1016/j.ijpharm.2009.05.058.
32. Hatfield SM, Kjaergaard J, Lukashev D, et al. Immunological mechanisms of the antitumor effects of supplemental oxygenation. *Sci Transl Med*. 2015;7(277):277ra30, doi:10.1126/scitranslmed.aaa1260.
33. Iijima M, Gombodorj N, Tachibana Y, et al. Development of single nanometer-sized ultrafine oxygen bubbles to overcome the hypoxia-induced resistance to radiation therapy via the suppression of hypoxia-inducible factor1alpha. *Int J Oncol*. 2018;52(3):679–686, doi:10.3892/ijo.2018.4248.
34. Khan MS, Hwang J, Lee K, et al. Anti-tumor drug-loaded oxygen nanobubbles for the degradation of hif-1alpha and the upregulation of reactive oxygen species in tumor cells. *Cancers (Basel)*. 2019;11(10):1464, doi:10.3390/cancers11101464.
35. Owen J, Logan K, Nesbitt H, et al. Orally administered oxygen nanobubbles enhance tumor response to sonodynamic therapy. *Nano Select*. 2021;3(2):394–401, doi:10.1002/nano.202100038.
36. Owen J, McEwan C, Nesbitt H, et al. Reducing tumour hypoxia via oral administration of oxygen nanobubbles. *PLoS One*. 2016;11(12):e0168088, doi:10.1371/journal.pone.0168088.
37. Song G, Ji C, Liang C, et al. TaOx decorated perfluorocarbon nanodroplets as oxygen reservoirs to overcome tumor hypoxia and enhance cancer radiotherapy. *Biomaterials*. 2017;112:257–263, doi:10.1016/j.biomaterials.2016.10.020.
38. Song R, Hu D, Chung HY, Sheng Z, Yao S. Lipid-polymer bilaminar oxygen nanobubbles for enhanced photodynamic therapy of cancer. *ACS Appl Mater Interfaces*. 2018;10(43):36805–36813, doi:10.1021/acsami.8b15293.

39. Song R, Peng S, Lin Q, et al. pH-Responsive oxygen nanobubbles for spontaneous oxygen delivery in hypoxic tumors. *Langmuir*. 2019;35(31):10166–10172, doi:10.1021/acs.langmuir.8b03650.
40. Tan H, Tian Y, Yang H, et al. Oxygen-sufficient lipid nanobubbles combined with UTMD for enhanced sonodynamic therapy of Hep-G2 cells. *J Biomed Mater Res B Appl Biomater*. 2021;109(11):1796–1806, doi:10.1002/jbm.b.34839.
41. Zhao M, Yang X, Fu H, et al. Immune/hypoxic tumor microenvironment regulation-enhanced photodynamic treatment realized by pH-responsive phase transition-targeting nanobubbles. *ACS Appl Mater Interfaces*. 2021;13(28):32763–32779, doi:10.1021/acsami.1c07323.
42. Gerling M, Zhao Y, Nania S, et al. Real-time assessment of tissue hypoxia in vivo with combined photoacoustics and high-frequency ultrasound. *Theranostics*. 2014;4(6):604–613, doi:10.7150/thno.7996.
43. Banche G, Allizond V, Mandras N, et al. Antimicrobial oxygen-loaded nanobubbles as promising tools to promote wound healing in hypoxic human keratinocytes. *Toxicol Rep*. 2022;9:154–162, doi:10.1016/j.toxrep.2022.01.005.
44. Khadjavi A, Magnetto C, Panariti A, et al. Chitosan-shelled oxygen-loaded nanodroplets abrogate hypoxia dysregulation of human keratinocyte gelatinases and inhibitors: new insights for chronic wound healing. *Toxicol Appl Pharmacol*. 2015;286(3):198–206, doi:10.1016/j.taap.2015.04.015.
45. Gupta S, Shende P. L-Proline adsorbed oxygen-loaded nanobubbles in-situ gel for wound healing. *Colloids Surf A Physicochem Eng Asp*. 2022;647:129028, doi:10.1016/j.colsurfa.2022.129028.
46. Bisazza A, Civra A, Donalisio M, Lembo D, Cavalli R. The in vitro characterization of dextran-based nanobubbles as possible DNA transfection agents. *Soft Matter*. 2011;7(22):10590–10593, doi:10.1039/c1sm06070h.
47. Afshari R, Akhavan O, Hamblin MR, Varma RS. Review of oxygenation with nanobubbles: possible treatment for hypoxic COVID-19 patients. *ACS Applied Nano Materials*. 2021;4(11):11386–11412, doi:10.1021/acsanm.1c01907.
48. Baram S, Weinstein M, Evans JF, et al. Drip irrigation with nanobubble oxygenated treated wastewater improves soil aeration. *Scientia Horticulturae*. 2022;291:110550, doi:10.1016/j.scienta.2021.110550.
49. Zhang H, Lyu T, Bi L, Tempero G, Hamilton DP, Pan G. Combating hypoxia/anoxia at sediment-water interfaces: a preliminary study of oxygen nanobubble modified clay materials. *Sci Total Environ*. 2018;637–638:550–560, doi:10.1016/j.scitotenv.2018.04.284.
50. Ebina K, Shi K, Hirao M, et al. Oxygen and air nanobubble water solution promote the growth of plants, fishes, and mice. *PLoS One*. 2013;8(6):e65339, doi:10.1371/journal.pone.0065339.
51. Sheskey PJ, Cook WG, Cable CG. *Handbook of pharmaceutical excipients*. London: Pharmaceutical Press; 2017.
52. Fayyaz M, Jabeen M, Tsipursky MS, Irudayaraj J. Dextran-based oxygen nanobubbles for treating inner retinal hypoxia. *ACS Applied Nano Materials*. 2021;4(7):6583–6593, doi:10.1021/acsanm.1c00084.
53. Zheng L, Wen Y, Ren W, Duan H, Lin J, Irudayaraj J. Hyperspectral dark-field microscopy for pathogen detection based on spectral angle mapping. *Sensors and Actuators B: Chemical*. 2022;367:132042, doi:10.1016/j.snb.2022.132042.
54. The United States Pharmacopeial Convention. *The United States Pharmacopeia: The National Formulary;* The United States Pharmacopeial Convention: Rockville, MD, USA, 2018.
55. Broderick C, Duncan L, Taylor N, Dick AA. INF-γ and LPS-mediated IL-10-dependent suppression of retinal microglial activation. *Invest Ophthalmol Vis Sci*. 2000;41(9):2613–2622.
56. Seigel GM, Sun W, Wang J, Hershberger DH, Campbell LM, Salvi RJ. Neuronal gene expression and function in the growth-stimulated R28 retinal precursor cell line. *Curr Eye Res*. 2004;28(4):257–269, doi:10.1076/ceyr.28.4.257.27831.
57. Sciarretta F, Fulci C, Palumbo C, et al. Glutathione transferase P silencing promotes neuronal differentiation of retinal R28 cells. *J Cell Physiol*. 2019;234(9):15885–15897, doi:10.1002/jcp.28246.
58. Seigel GM, Yuan K, Goldsmith ZK, Morales-Tirado VM. Heterogeneous R28 retinal precursor cells predominantly express retinal ganglion cell and glial cell markers. *Invest Ophthalmol Vis Sci*. 2018;59(9):4592–4592.
59. Putsylnikov S, Sagar D, Jain P, Khan ZK. Targeting the C-type lectins-mediated Host-Pathogen interactions with dextran. *J Pharmacy Pharm Sci*. 2014;17(3):371–392, doi:10.18433/J3N590.
60. Thakur SS, Ward MS, Popat A, et al. Stably engineered nanobubbles and ultrasound - an effective platform for enhanced macromolecular

delivery to representative cells of the retina. *PLoS One*. 2017;12(5):e0178305, doi:10.1371/journal.pone.0178305.
61. Thakur SS, Chen YS, Houston ZH, et al. Ultrasound-responsive nanobubbles for enhanced intravitreal drug migration: an ex vivo evaluation. *Eur J Pharm Biopharm*. Mar 2019;136:102–107, doi:10.1016/j.ejpb.2019.01.014.
62. Beltrán-Gracia E, López-Camacho A, Higuera-Ciapara I, Velázquez-Fernández JB, Vallejo-Cardona AA. Nanomedicine review: clinical developments in liposomal applications. *Cancer Nanotechnol*. 2019;10(1), doi:10.1186/s12645-019-0055-y.
63. Jin J, Yang L, Chen F, Gu N. Drug delivery system based on nanobubbles. *Interdisciplinary Materials*. 2022;1(4):471–494, doi:10.1002/idm2.12050.
64. Zarrintaj P, Saeb MR, Jafari SH, Mozafari M. Application of compatibilized polymer blends in biomedical fields. *Compatibilization of Polymer Blends*. 2020:511–537.
65. Dias AMA, Freire M, Coutinho JAP, Marrucho IM. Solubility of oxygen in liquid perfluorocarbons. *Fluid Phase Equilibria*. 2004;222–223:325–330, doi:10.1016/j.fluid.2004.06.037.
66. Wang W, Cheng Y, Yu P, et al. Perfluorocarbon regulates the intratumoural environment to enhance hypoxia-based agent efficacy. *Nat Commun*. 2019;10(1):1580, doi:10.1038/s41467-019-09389-2.
67. Kim JY, Song MG, Kim JD. Zeta potential of nanobubbles generated by ultrasonication in aqueous alkyl polyglycoside solutions. *J Colloid Interface Sci*. 2000;223(2):285–291, doi:10.1006/jcis.1999.6663.
68. Basilico N, Magnetto C, D'Alessandro S, et al. Dextran-shelled oxygen-loaded nanodroplets reestablish a normoxia-like pro-angiogenic phenotype and behavior in hypoxic human dermal microvascular endothelium. *Toxicol Appl Pharmacol*. 2015;288(3):330–338, doi:10.1016/j.taap.2015.08.005.
69. Bessone F, Argenziano M, Grillo G, et al. Low-dose curcuminoid-loaded in dextran nanobubbles can prevent metastatic spreading in prostate cancer cells. *Nanotechnology*. 2019;30(21):214004, doi:10.1088/1361-6528/aaff96.
70. Prato M, Khadjavi A, Magnetto C, et al. Effects of oxygen tension and dextran-shelled/2H,3H-decafluoropentane-cored oxygen-loaded nanodroplets on secretion of gelatinases and their inhibitors in term human placenta. *Biosci Biotechnol Biochem*. 2016;80(3):466–472, doi:10.1080/09168451.2015.1095068.
71. Prato M, Magnetto C, Jose J, et al. 2H,3H-decafluoropentane-based nanodroplets: new perspectives for oxygen delivery to hypoxic cutaneous tissues. *PLoS One*. 2015;10(3):e0119769, doi:10.1371/journal.pone.0119769.
72. Zhuge D, Li L, Wang H, et al. Bacterial toxin-responsive biomimetic nanobubbles for precision photodynamic therapy against bacterial infections. *Adv Healthc Mater*. 2022;11(18):e2200698, doi:10.1002/adhm.202200698.
73. Cavalli R, Bisazza A, Giustetto P, et al. Preparation and characterization of dextran nanobubbles for oxygen delivery. *Int J Pharm*. 2009;381(2):160–165, doi:10.1016/j.ijpharm.2009.07.010.
74. Jones CI, Payne DA, Hayes PD, et al. The antithrombotic effect of dextran-40 in man is due to enhanced fibrinolysis in vivo. *J Vasc Surg*. 2008;48(3):715–722, doi:10.1016/j.jvs.2008.04.008.
75. Bhandari P, Wang X, Irudayaraj J. Oxygen nanobubble tracking by light scattering in single cells and tissues. *ACS Nano*. 2017;11(3):2682–2688, doi:10.1021/acsnano.6b07478.
76. Chen Z, Liu L, Liang R, et al. Bioinspired hybrid protein oxygen nanocarrier amplified photodynamic therapy for eliciting anti-tumor immunity and abscopal effect. *ACS Nano*. 2018;12(8):8633–8645, doi:10.1021/acsnano.8b04371.
77. Magnetto C, Prato M, Khadjavi A, et al. Ultrasound-activated decafluoropentane-cored and chitosan-shelled nanodroplets for oxygen delivery to hypoxic cutaneous tissues. *RSC Adv*. 2014;4(72):38433–38441, doi:10.1039/c4ra03524k.
78. Han X, Jeong Y, Irudayaraj J. Nanocatalase-based oxygen-generating nanocarriers for active oxygen delivery to relieve hypoxia in pancreatic cancer. *ACS Applied Nano Materials*. 2022;5(11):17248–17257, doi:10.1021/acsanm.2c04241.